

Effect of the fabrication method on the functional properties of BaTiO₃: PVDF nanocomposites

Alessandro Chiolerio · Mariangela Lombardi · Andrea Guerriero · Giancarlo Canavese · Stefano Stassi · Rossana Gazia · Valentina Cauda · Diego Manfredi · Angelica Chiodoni · Alessio Verna · Matteo Cocuzza · Laura Montanaro · Candido Fabrizio Pirri

Received: 17 March 2013 / Accepted: 1 June 2013 / Published online: 14 June 2013
© Springer Science+Business Media New York 2013

Abstract This paper deals with the preparation and characterization of nanocomposite (NC) materials, comparing different technologies for sample fabrication, in view of their possible application as piezoelectric sensors. Those NCs consist on BaTiO₃ nanoparticles embedded into a polyvinylidene fluoride matrix, where both the ceramic and the polymeric phases could exhibit ferroelectricity. In particular, we compare the properties of samples prepared through three different methods, i.e., solvent casting, enabling a fast realization, spin-coating, which allows to realize thin flexible films particularly interesting for large area sensors, and hot embossing, which is exploited to modify the residual porosity in the thick films. The influence of the fabrication techniques on the physical and chemical properties is investigated. Different electrode materials have been tested and compared, ranging from sputtered Pt to an engineered thermally evaporated Ti/Au bilayer. Leakage current, polarization, displacement curves, and piezoelectric coefficient d_{33} are evaluated by small signal indirect measurements, comparing the properties of different materials and understanding how processing technologies influence the sensor performances by acting on the functional materials.

Introduction

Piezoelectric materials are able to couple electric polarization and mechanical displacements and for this capability they are often used in technological applications such as sensors or actuators [1, 2]. In particular, the direct piezoelectric effect is widely exploited in sensing devices: when it is mechanically stressed, a piezoelectric material undergoes a change in its polarization. The direct piezoelectric effect can be written as:

$$D_i = d_{ij}\sigma_j \quad (1)$$

In Eq. (1) D_i is the dielectric displacement, σ_j is the applied stress, and d_{ij} is the piezoelectric coefficient, while the subscripts i and j identify the generic i th or j th direction. Considering the polarization of a planar sample along the out-of-plane direction, generally in a piezoelectric device mechanical strain and electric field are parallel to this direction. For this reason the functional behavior of a piezoelectric material is measured through the evaluation of its longitudinal piezoelectric coefficient, d_{33} [2].

As concerns piezoelectric sensors, being these devices aimed at producing dielectric displacement in response of mechanical stresses, it is evident that a high d_{33} value is desirable and this explains the relevant exploitation in this field of piezoceramics, particularly of lead–zirconate–titanate materials (PZT). Some polymers, as polyvinylidene fluoride (PVDF), can also show the same behavior, but their piezoelectric properties are smaller with respect to ceramics: mean d_{33} values of about +450 and –25 pC/N are in fact found for PZT and PVDF, respectively [3]. For certain applications BaTiO₃ (BT) is preferred to PZT as inorganic filler for its environmentally friendly nature and ease in handling, as Pb-free material. Notwithstanding the

A. Chiolerio (✉) · M. Lombardi · G. Canavese · S. Stassi · R. Gazia · V. Cauda · D. Manfredi · A. Chiodoni · A. Verna · M. Cocuzza · L. Montanaro · C. F. Pirri
Istituto Italiano di Tecnologia, Center for Space Human Robotics, Corso Trento 21, 10129 Torino, Italy
e-mail: alessandro.chiolerio@iit.it

M. Lombardi · A. Guerriero · M. Cocuzza · L. Montanaro · C. F. Pirri
Applied Science and Technology Department, Politecnico di Torino, Corso Duca degli Abruzzi 24, 10129 Torino, Italy

worse functional features, PVDF presents all the advantages of polymeric materials, such as low densities and low costs, as well as good workability, easy maintenance and repair, and recycling capabilities typical of thermoplastics [4, 5]. The limited piezoelectric properties and the flexibility necessary to conform to the substrate surface make PVDF and its copolymers promising candidates for large area tactile sensors [4].

The piezoelectric properties of PVDF materials can be improved exploiting them as matrices in composites [6], in which piezoelectric ceramics with different composition and morphology are added. Among the several possibilities, 0–3 composites can be prepared by dispersing piezoelectric ceramic particles in PVDF. Such materials are characterized by ceramic particles not in contact with each other, thus having connectivity 0, dispersed in a continuous polymeric network, having connectivity 3 [7]. The 0–3 composites may couple the easy processability and mechanical flexibility typical of polymers with the higher piezoelectric coefficient and huge dielectric constant of the ceramic filler. Besides the connectivity, the composite properties are strictly influenced by the composition of the two phases, their volume fraction and the processing method used for their preparation [8]. Generally, this type of composites can be prepared through solvent casting [9], spin coating [10] and/or hot pressing [11]/compression molding [12] under specific conditions [8, 13]. For example, solvent casting must be carried out taking care of removing the solvent residues or residual porosities [8]. This drawback may be overcome through an annealing procedure, strictly controlling the experimental conditions to increase the material density, or hot pressing/compression molding of the solvent cast films [8].

In this paper 0–3 composites obtained by adding a high amount of BT nanoparticles (NPs) in a PVDF matrix are described, investigating the relationship between the material processing and their functional properties. We underline the fact that BT has a mean d_{33} value of 190 pC/N [14].

The expected result for these nanocomposites (NCs) is to realize conformable skins with a suitable functional response. The choice of this connectivity could be a solution to realize a conformable sensor for complex mechanical frames. This study consists in a preliminary investigation about the preparation and processing of piezoelectric composites, in view of the development of sensing skins for robotic structures, already studied using piezoresistive devices [15]. In this case, a current flow is systematically measured across the material, raising some power management issues that a piezoelectric composite does not introduce, since the charge is accumulated through mechanical displacement and must simply be measured. In the configuration here proposed (piezoelectric hybrid) no

current generators are needed and ultra low power devices could be used for the signal readout.

Materials and methods

Preparation of piezoelectric hybrids

Commercial PVDF (Kynar 720[®], Arkema[®], density 1.78 g/cm³, melting point 168 °C, T_g –40 °C) pellets were dissolved in dimethylformamide (DMF, Sigma Aldrich) under magnetic stirring at 60 °C for 60 min. A fixed amount of BT NPs (BT, Inframat Advanced Materials, mean size of 500 nm) was then added into the polymer solution to reach a solid amount of 400 phr (per hundred resin), corresponding to 80 wt% or 55 vol%. The NC formulation was then homogenized with a high speed shear-based mechanical mixing (Ultra-Turrax) at 30000 rpm for 5 min and used for producing films through the solvent casting (SC) or the spin-coating (SpC) techniques. In particular, thick films were produced by casting PVDF–BT mixture in a glass Petri dish, whereas thin films were obtained by spin-coating the organic–inorganic formulation at 3000 rpm for 10 s. A flow-chart of the preparation process is shown in Fig. 1.

The SpC and SC samples were then submitted to the solvent evaporation in a closed system at 60 °C for 3 or 24 h, respectively.

SC samples were then pressed at high temperature in a hot embossing system, producing the HE samples. Our equipment is the HEX01 hot embossing system from JENOPTIK Mikrotechnik, which basically is a tool able to produce and maintain simultaneously a high pressure and a

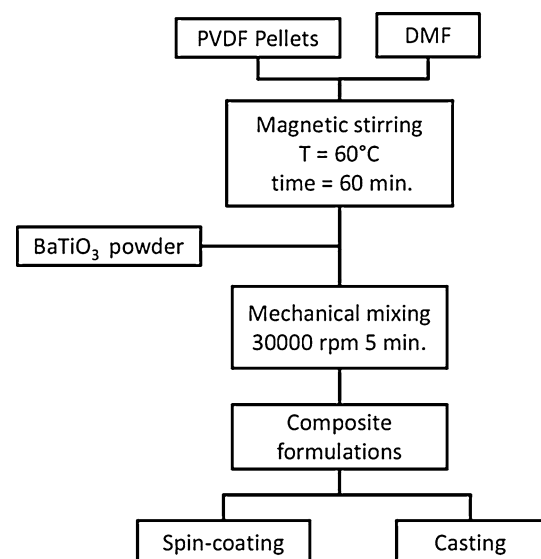


Fig. 1 Flow-chart of the preparation method

reasonably high temperature between two steel plates. Four samples with surface area of 1 cm^2 were embossed at $2 \times 10^8 \text{ Pa}$ (20 kN). We tested the following configurations: $100 \text{ }^\circ\text{C}$ for 5 min, $100 \text{ }^\circ\text{C}$ for 10 min, $150 \text{ }^\circ\text{C}$ for 5 min, and $150 \text{ }^\circ\text{C}$ for 10 min. This choice of parameters has been made to treat the samples at the most extreme conditions available for our hot embossing device. The effective value of applied pressure may not be as high as the nominal one but could be lower due to extreme stiffness given by the ceramic component of the NCs [16–19].

Structural and morphological characterization

The ceramic NPs were characterized by granulometric analysis (Fritsch model Analysette 22 Compact) and Scanning Electron Microscopy (SEM, Hitachi 2300), in order to evaluate their size distribution and agglomeration state (Figs. 2, 3).

The composite films were characterized in terms of composition through X-ray diffraction (XRD, Philips PW 1710, in the range 2θ $5\text{--}70^\circ$, with a step size of 0.05° and an acquisition time per step of 5 s) and FTIR (Thermo Nicolet 5700, in the range $4000\text{--}400 \text{ cm}^{-1}$, with a spectral resolution of 2 cm^{-1}) and their microstructures were evaluated by Field Emission Scanning Electron Microscopy (FESEM, Zeiss Supra 40).

Top and bottom electrodes for functional characterization

Two different conductive substrates were used as bottom electrodes (with a flat rectangular shape) to test the functional properties: a standard low cost printed circuit board (PCB, resin coated by a thick copper layer, rough surface), or an atomically-flat gold-coated silicon wafer. Bottom electrodes together with their substrates were also used to guarantee a mechanical support for the functional measurements. Functional characterization of piezoelectric hybrids was carried out using atomically-flat gold-coated

silicon wafers only, since the high surface roughness of standard PCBs led to a local intensification of the electric field often resulting in sample breakdown.

Top electrodes were always structured according to the functional measurement setup, using a shadow masking stencil that reproduced several circular patterns onto the sample surface, having areas ranging from 1 to 10 mm^2 (see further Fig. 4d). We used two different nanostructured layers: a sputtered Pt thin film and a thermally evaporated Ti/Au bilayer, testing their readiness for practical applications.

Pt thin films were deposited with a Q150TES (Quorum Technology) sputtering system, operating at 50 mA for 180 s at room temperature and 8×10^{-4} mbar vacuum level. The nominal thickness of Pt electrodes was 50 nm.

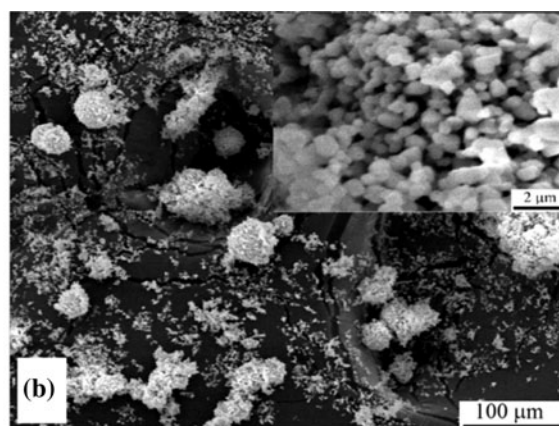
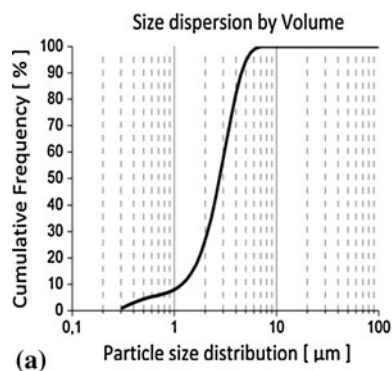
For the evaporation of the Ti/Au top electrodes, a thermal evaporator was used, equipped with three crucibles, one for Ti and two for Au. The current and the time set for the evaporation of Ti and Au were of 170 A for 30 s, and 120 A for 570 s, respectively. The thicknesses of the Ti layer and the Au layer were 5 and 200 nm, respectively.

All thicknesses here indicated (sputtered Pt, evaporated Ti and Au) are nominal values, resulting from a common calibration procedure that is performed measuring with a mechanical tip profilometer a certain number of films grown in the same conditions varying the deposition time and extrapolating an empirical calibration function (thickness: dependent variable, time: independent variable).

Functional characterization

Current–voltage (I–V) curves, polarization hysteresis loops, capacitive measures, and piezoelectric butterflies were collected for each sample by a piezo evaluation system (PES, TFAalyzer 2000HS, Aixact) coupled to a single point laser vibrometer (Polytec OVF-505). The system exploits the converse piezoelectric effect (i.e., generation of a mechanical displacement under the application of an electric field). All the measurements were performed applying a triangular

Fig. 2 **a** Particle size distribution and **b** SEM micrographs of the as-received BT powder



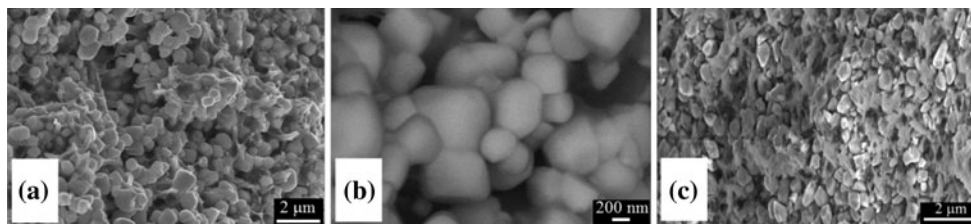


Fig. 3 **a, b** FESEM micrographs of the PVDF–BT SC composites (very similar to SpC sample) **c** HE sample (150 °C, 10 min)

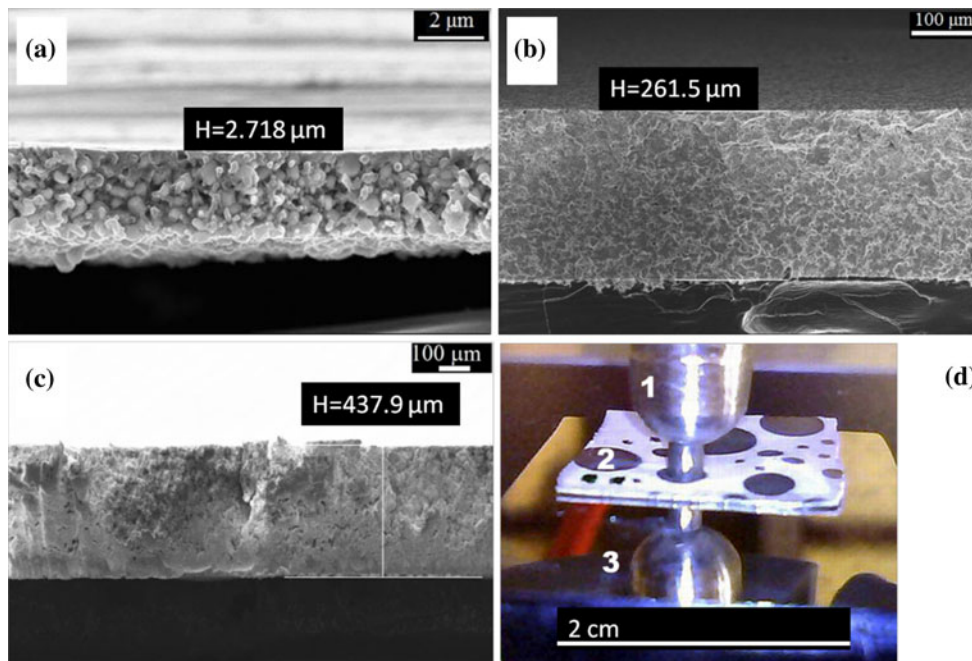


Fig. 4 FESEM images of the cross sections of the **a** SpC, **b** SC, and **c** HE PVDF–BT films. **d** Optical image showing the functional characterization setup: **1** top electrode integrating the laser

interferometer; **2** top contacts thermally evaporated/sputtered on the NC hybrid slab, in this case a HE sample; **3** bottom electrode realized by means of thermally evaporated Ti/Au on monocrystalline silicon

voltage signal with variable frequency and amplitude depending on the kind of sample. For the capacitive and d_{33} characterization a sinusoidal voltage signal with a frequency in the kHz range was superimposed to the triangular stimulus. This method, allowing a more precise measurement of the piezoelectric coefficients, is called small signal technique since the sinusoidal voltage signal is ~ 50 times bigger with respect to the triangular one [20].

After the piezoelectric characterization, each sample was observed by FEG-SEM.

Results

Sample characterization

Even if the supplier declared a mean diameter of 500 nm, the granulometric analysis of the as-received BT powder, reported in Fig. 2a, revealed a micrometric particle size

distribution: in fact, d_{10} , d_{50} , and d_{90} values of 1.4, 3.4, and 6.5 μm were found.

SEM observations of the as-received powder (Fig. 2b) showed large agglomerates, in which the NPs, with diameters comparable with the value claimed by the supplier, were identified (see the inset of Fig. 2b).

Even if a relevant agglomeration was present in the as-received powder, BT NPs were homogeneously distributed in the PVDF composites, as illustrated in Fig. 3. The final microstructure was not influenced by the deposition method: in fact, both SC and SpC samples presented a homogeneous distribution of the ceramic particles, with some agglomerates in which the polymeric matrix was not able to completely infiltrate. In panel (a) and (b), the SC sample is shown in two different magnification scales, also representing SpC samples whose morphology is pretty similar. As shown in panel (c), the dispersion of NPs did not change also after hot embossing at the maximum temperature (150 °C, 10 min).

In order to analyze the cross-sections and measure each sample thickness, fragile breaking was used by submitting the composites to liquid nitrogen, which brings the material below the glass transition temperature of PVDF ($-40\text{ }^{\circ}\text{C}$ for the pure matrix). As a consequence of the method employed for their production, HE, SpC, and SC films had a thickness in the range 200–400, 3–7, and 250–450 μm , respectively, as stated by FESEM observation of their cross sections (Fig. 4). Residual porosity, estimated by the analysis of FESEM sections, may be given as follows: SC 1.80 %, SpC 1.90 %, HE 0.60 %. In particular this was done by thresholding the images, transforming the grayscale in a 2-bit-valued image, and applying a specific algorithm for thresholded areas recognition able to output the diameter distribution and number of the pores exposed to the fracture section [21, 22]. Only round-shaped pores are evaluated by the algorithm, since polygonal pores may result from detachment of ceramic particles during sample fragile breaking. These results demonstrated that the casting procedures had a negligible effect on the final microstructure of the PVDF–BT composites (by comparing SC and SpC samples), whereas the pressure assisted method at high temperatures optimized the packing of the organic–inorganic systems.

The presence of the piezoelectric phase for inorganic and organic components of these composites were confirmed by XRD analysis (Fig. 5a) and by FTIR measurements (Fig. 5b), respectively.

In particular, XRD patterns of all the samples (SC, SpC, and HE materials) mainly showed the BT peaks, having a very high intensity with respect to those of the PVDF, being the matrix volume very limited in the NCs and partially crystalline. This characterization allowed to assess the tetragonality of the BT particles (JCPDS #05-0626) in all the samples. On the other hand, the FTIR measurements

carried out on the film surfaces, detected the signals of the α - and γ -phases (see peaks at 765 cm^{-1} for the former, at 812 and 431 cm^{-1} for the latter) in the case of the pure polymer.

The piezoelectricity of PVDF depends on its crystalline phase: among the different ones (called α , β , γ , δ), only the β -phase shows the best ferroelectric and piezoelectric properties. The order degree of PVDF (hence its crystalline phase) depends on the processing conditions: melt blending induces the crystallization of the α -phase, whereas solution blending favors the β one, mainly if the solvent evaporation was carried out at temperatures lower than $70\text{ }^{\circ}\text{C}$ [1, 23, 24]. The piezoelectric phase of PVDF can be also obtained through mechanical stretching or incorporation of some additives [1, 23].

In the PVDF–BT cast materials (both SC and SpC samples) the β -phase was predominant, as expected on the basis of the temperature chosen for the solvent evaporation ($60\text{ }^{\circ}\text{C}$) [24]. In addition, the inorganic particles seem to slightly favor the crystallization of the β -phase, being the signal of the α -phase absent in SC and SpC composites. This could be due to the ability of the ceramic particles to behave as nucleating agents in the crystallization phenomena of polymeric matrices, in particular for the β -phase in the case of PVDF [23]. On the other hand, in the HE samples an increasing presence of the α -phase was detected when the treatment temperature raised, in agreement with the phase transition conditions [23].

Evaluation of sample performances

Functional characterization was performed on all samples, showing that a substantial piezoelectric response was measurable only in certain cases, in particular for HE and SC samples. SpC samples were such that their lower

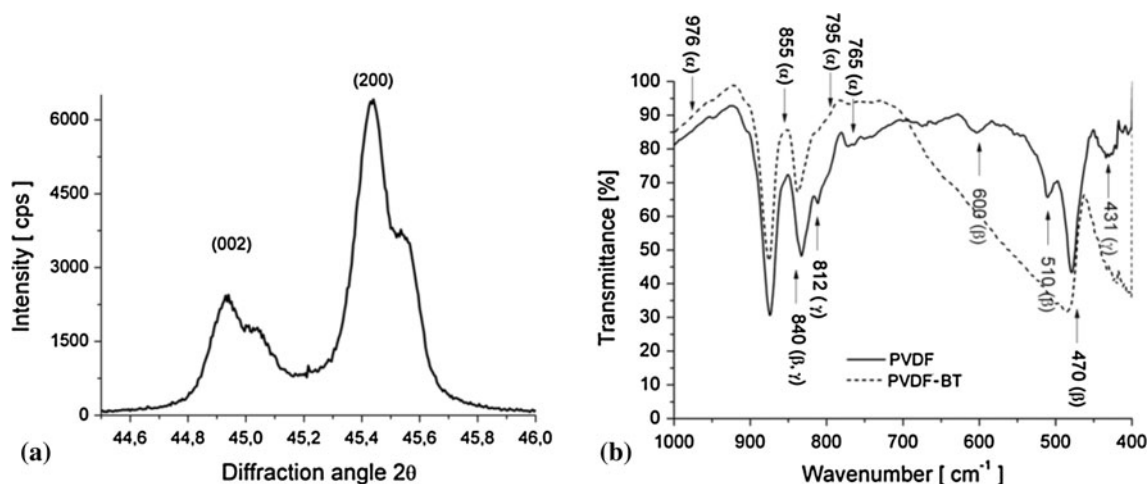


Fig. 5 **a** XRD pattern of PVDF–BT SC composites (very similar to SpC and HE samples) and **b** FTIR spectra of the same material (*continuous line*) compared to that of pure PVDF matrix (*dashed line*)

thickness resulted in a substantial statistical probability of percolative tracks or pinholes, giving rise to preferential current flows and easy breakdown. The same breakdown was easily produced by electric field enhancement on the bottom surface placed in contact with standard Cu-coated PCBs, hence the final choice for functional characterization (results shown in Figs. 6, 7, 8, 9) converged upon Au-coated Si wafers and Ti/Au evaporated layers, as will be explained in “Evaluation of top electrode toughness” section. Figure 6a shows IV curves, normalized to electric field and current density by considering the sample geometries reported in Table 1. It is possible to notice a strong effect due to sample preparation: the most effective response, showing a good trade-off between loss (curve area) and linearity (discrepancy between linear response and experimental curve), is seen for the SC sample, while the SpC one features higher nonlinearity and the HE one results in an enhanced conductivity (see values reported in Table 1). In particular the highest the linearity the lowest the resistivity of the sample. Figure 6b reports displacement curves measured in similar conditions on the three samples, evidencing a higher displacement on HE samples in comparison to samples prepared by other techniques, even though we will show in the following explanation that displacement is not due to piezoelectricity. On the contrary SpC samples showed no measurable displacement, probably in relation to their extremely flexible nature; in the following analyses we decided hence to focus on HE and SC samples, those that featured an active response.

Figure 7 presents a comparison between different excitation signal frequencies submitted to HE samples, in particular showing: the electric response in form of JE curves in panel (a), computed from standard IV measures after taking into account sample geometry; the polarization in panel (b); the mechanical displacement along the out-of-plane direction versus the electric field strength (applied on

the same direction) in panel (c). Typically HE samples show quite high leakage currents, no hysteresis of the polarization curves (non ferroelectric response) and a displacement behavior that might be addressed as piezoelectric. We found a strong dependency of the displacement on the measurement frequency, i.e., a progressive reduction of the actuation efficiency when increasing the excitation signal frequency, clear indication of the fact that the displacement may be ascribed to electrostriction [25]. Electrostriction is caused by the presence of randomly aligned electrical domains in all dielectrics, whose polarization induced by the measurement setup produces attractive forces, hence a deformation of the sample. Electrostriction is a quadratic effect, proportional to the square of electric polarization. On the contrary piezoelectricity is a linear effect and does not apply to all dielectrics. The frequency analysis confirms this, since the piezoelectric effect is not dependent on the excitation signal frequency within a reasonable range like the one proposed in our characterizations (see further in the text, Fig. 8). So sample HE is neither ferroelectric nor piezoelectric.

Figure 8 shows the same plots of Fig. 7, related to the SC sample tested in a similar range of frequencies. SC samples showed a very slight dependence upon measurement frequency, as shown in panel c), proof of a genuine piezoelectric effect; also a slight asymmetry in the butterfly diagram of the displacement curve was found. By comparing panels (a) of both Figs. 7 and 8 it is possible to notice as well that the current density flowing through HE samples is an order of magnitude higher than that measured through SC samples, while the electric field range is on the same order of magnitude. As a consequence, polarization curves in panel (b) become more dissipative (round-shaped, Fig. 7, low frequency) for HE samples, while for SC samples we could measure a minor hysteresis loop typical of a ferroelectric system. The displacement

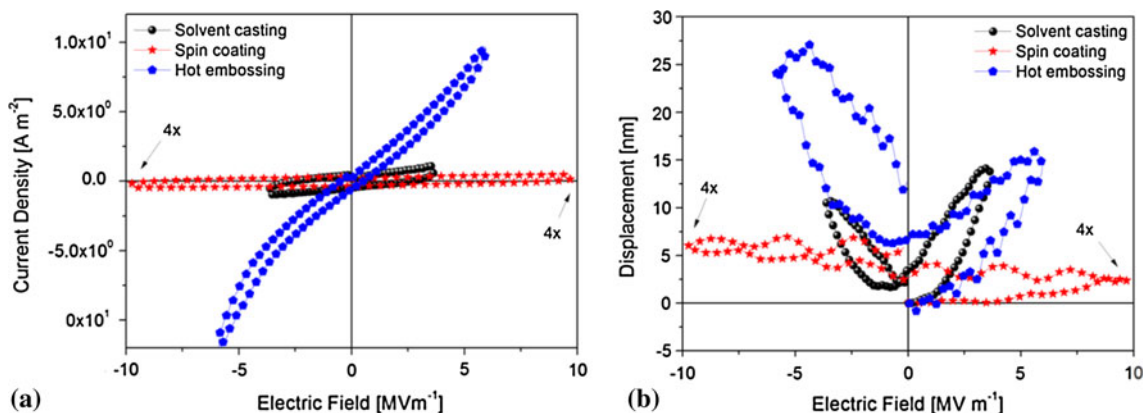


Fig. 6 **a** IV curve measurements performed at 10 Hz on HE, SpC, and SC samples, **b** corresponding displacement curves. Please note that the horizontal axis in both graphs for sample SpC has been shrunk four times to facilitate data comparison

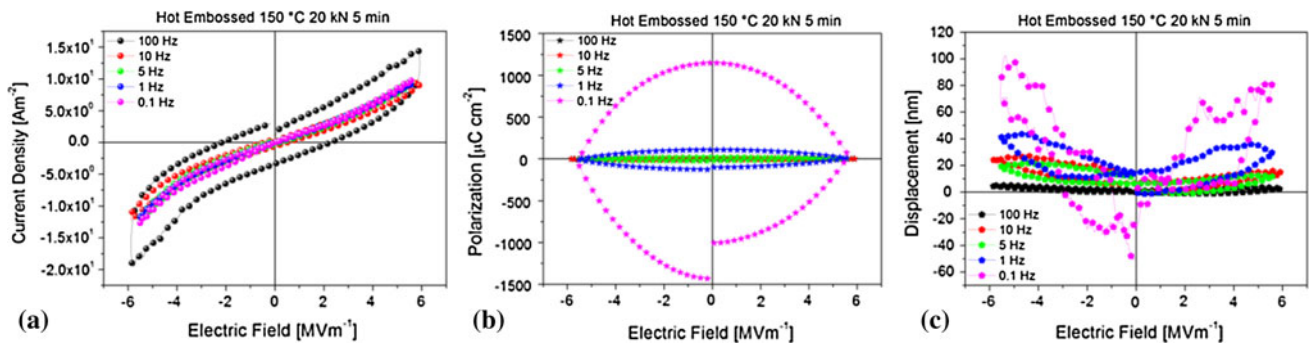


Fig. 7 **a** IV curves performed at different frequencies on HE samples (150 °C 20 kN for 5 min), given in form of JE curves by taking into account sample geometry; **b** corresponding polarization curves, **c** corresponding displacement curves

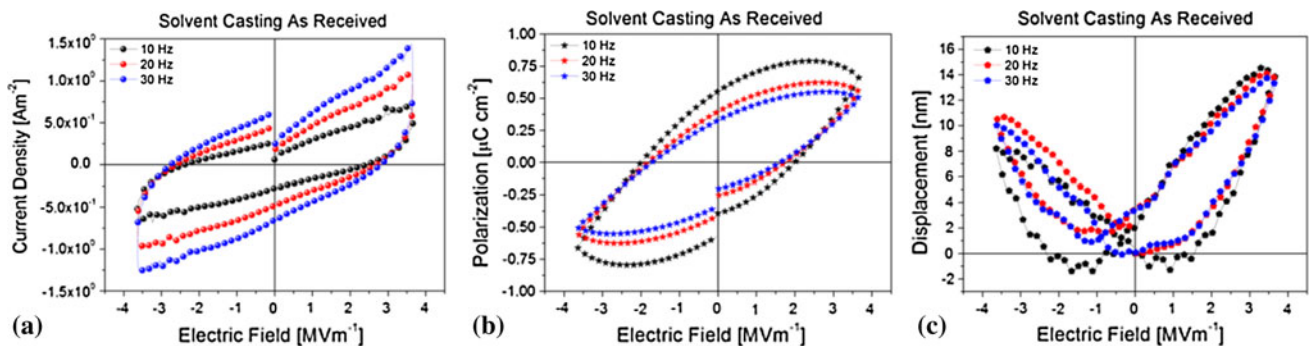


Fig. 8 **a** IV curves given in form of JE curves by taking into account sample geometry, performed at different frequencies on the solvent casted samples, containing BT NPs as received, **b** corresponding polarization curves, **c** corresponding displacement curves

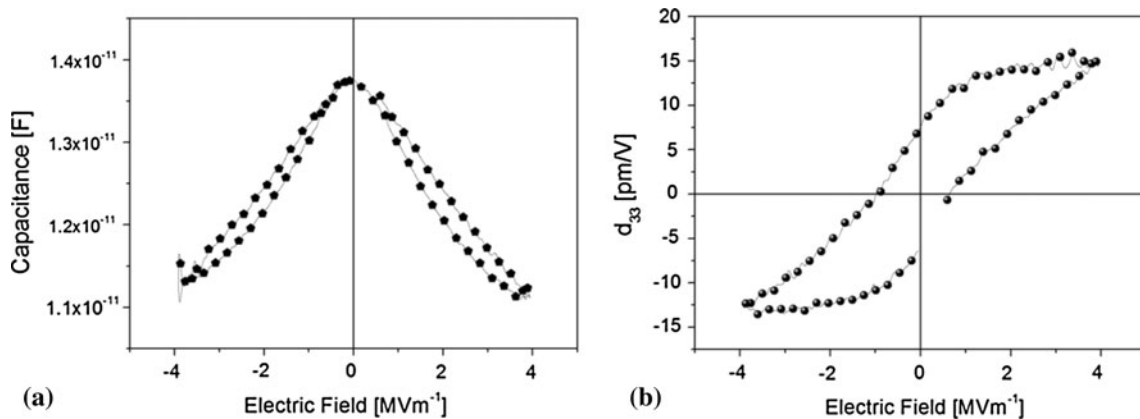


Fig. 9 **a** Capacitance curve on SC sample, **b** corresponding d_{33} curve

Table 1 Geometrical and functional properties of the BT–PVDF NCs

Sample	Porosity (%)	Thickness (μm)	Electrode area (mm ²)	Linearity IV curve (–)	Resistivity (MΩ m)	Loss (MW m ⁻³)	d_{33} (pm V ⁻¹)
SC	1.80	350	7	0.424	5.869	5.965	15
SpC	1.90	5	5	0.201	160.3	43.08	N/A
HE	0.60	300	1.75	0.969	0.6559	14.36	N/A

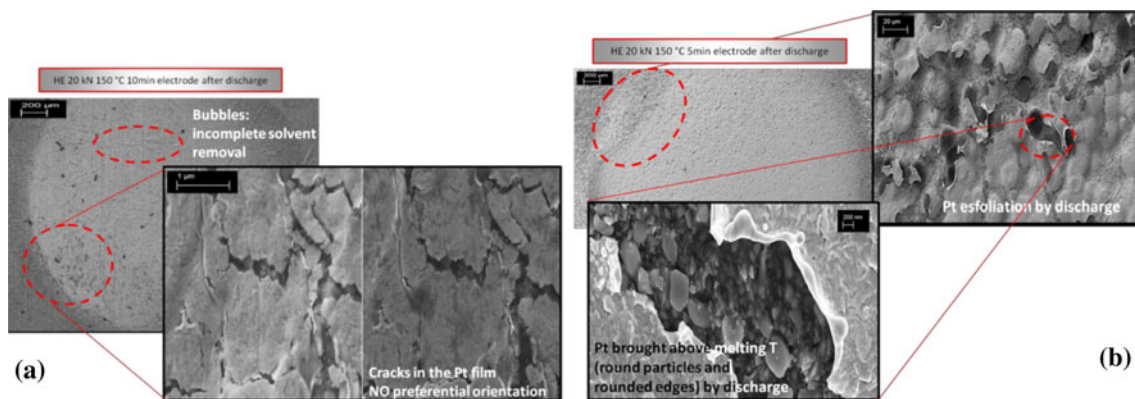


Fig. 10 **a** FESEM images showing sputtered Pt top electrode on HE sample after PES functional characterization: crack formation and bubble formation, **b** local melting and exfoliation after breakdown

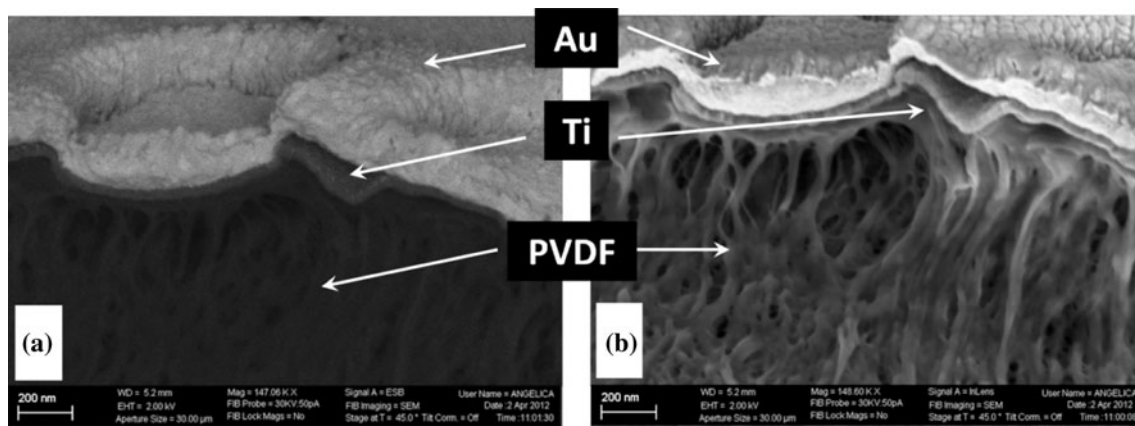


Fig. 11 FESEM image (backscattered electrons on the *left* and secondary electrons on the *right*) showing thermally evaporated Ti/Au top electrode on PVDF sample after PES functional characterization

butterfly curve in panel (c) confirms that sample SC is both ferroelectric and piezoelectric.

Considering that it was not possible to measure a displacement above mechanical noise for SpC samples (minimum displacement > 1 nm) and that we found the displacement was produced by electrostrictive effects for HE samples, we tested the small signal performances only for SC samples, obtaining a mean d_{33} around 15 pm/V, as shown in Fig. 9b.

Such a value, closer to the typical response of PVDF than to the response of a BT bulk ceramic, indicates that the role of the filler in the NC is purely ferroelectric. On the contrary the matrix is both ferroelectric and piezoelectric in SC samples and purely dielectric in HE samples, due to an increase of the α -phase content induced by the high processing temperatures. SpC samples, unfortunately, are such that no piezoelectric answer could be measured.

Evaluation of top electrode toughness

Since hybrid piezoelectric materials should produce substantial volume variation, it is fundamental to characterize the morphology of the electrodes and assess their plasticity. Figure 10 shows some failures in a sputtered Pt electrode, whose rigidity does not allow accommodation and results in crack formation. Those cracks and some local melting were found on top electrodes after sample failure due to electrical breakdown, as a consequence of functional characterization.

On the contrary, thermally evaporated Ti/Au bilayer features a higher plasticity and is able to accommodate sample displacement and permanent deformation, as shown in Fig. 11 on a PVDF sample without any filler. A certain detachment is found between the outer Au film and the Ti adhesion promoter but this was produced during sample breaking for section characterization.

All functional measurements discussed in “[Evaluation of sample performances](#)” section have been obtained with the best choice of Ti/Au top electrodes.

Conclusions

In conclusion, we compared the functional properties of three different, largely available and versatile techniques for sample structuring toward the realization of a sensing skin. Spin-coating results in extremely thin samples, too flexible to produce a measurable response with our equipment; hot-embossed samples resulted quite brittle, inadequate for a conformable device; solvent casting, the simplest technique, produced functional and flexible membranes which we found suitable for the proposed applications.

Considering the experimental results we can conclude that: the NPs distribution within the matrix of the composites was optimal; a very low residual porosity could be reached, in each case below 2 % and in the best case 0.60 % (HE samples). Pt electrodes were too fragile to be compliant with the system and evidence some electrical breakdown. A convenient choice was found in thermally evaporated Ti/Au. We can conclude that a real piezoelectric/ferroelectric response was found for SC samples (around 15 pm/V). Leakage currents in HE samples were quite large, possibly due to direct connection between NPs; functional measurements showed the occurrence of electrostrictive phenomena. Dielectric strength in SpC samples was not high enough to produce a sufficiently high response to be measurable.

A possible improvement of functional properties/processing ease/toughness is reachable through NP functionalization, enhancing both the electrical and the mechanical links between filler and matrix.

References

- Cardoso VF, Costa CM, Minas G, Lanceros-Mendez S (2012) *Smart Mater Struct* 21:085020
- Aksel E, Jones JL (2010) *Sensors* 10:1935
- Richardson PD (1989) *IEEE Eng Med Biol Mag* 8:14
- Seminara L, Pinna L, Valle M, Basiricò L, Cosseddu P, Bonfiglio A, Ascia A, Biso M, Ansaldo A, Ricci D, Metta G (2012) Piezoelectric polymer transducer arrays for flexible tactile sensors. In: *IEEE SENSORS proceedings*, Taipei Taiwan, 28–31 October 2012
- Kwak SB, Nam JD (2002) *Polym Eng Sci* 42:1674
- Capsal JF, Dantras E, Laffont L, Dandurand J, Lacabanne C (2010) *J Non-Cryst Solids* 356:629
- Newnham RE, Skinner DP, Cross LE (1978) *Mater Res Bull* 13:525
- Dalle Vacche S, Oliveira F, Leterrier Y, Michaud V, Damjanovic D, Manson J-AE (2012) *J Mater Sci* 47:4763. doi:[10.1007/s10853-012-6362-x](https://doi.org/10.1007/s10853-012-6362-x)
- Chan HLW, Zhang QQ, Ng WY, Choy CL (2000) *IEEE Trans Dielectr Electr Insul* 7:204
- Dietze M, Krause J, Solterbeck CH, Es-Souni M (2007) *J Appl Phys* 101:054113
- Mao YP, Mao SY, Ye ZG, Xie ZX, Zheng LS (2010) *J Appl Phys* 108:014102
- Chan HLW, Chan WK, Zhang Y, Choy CL (1998) *IEEE Trans Dielectr Electr Insul* 5:505
- Wegener M, Arlt K (2008) *J Phys D* 41:165409
- Vijatović MM, Bobić JD, Stojanović BD (2008) *Sci Sinter* 40:235
- Crepaldi M, Chiolerio A, Tommasi T, Hidalgo D, Canavese G, Stassi S, Demarchi D and Pirri CF (2013) A low complexity wireless microbial fuel cell monitoring using piezoresistive sensors and impulse-radio ultra-wide-band. In: *SPIE proceedings* 8763-33
- Becker H, Heim U (2000) *Sensors Actuators A* 83:130
- Arbatti M, Shan X, Cheng Z-Y (2007) *Adv Mater* 19(10):1369
- Wang J, Wang YE, Li S, Xiao J (2010) *J Polym Sci B* 4:490
- Wang G, Deng Y, Guo L (2010) *Chem Eur J* Vol 16 33:10220
- Gerber P, Kügeler C, Böttger U, Waser R (2004) *J Appl Phys* 95(16):4976
- Virga A, Rivolo P, Descrovi E, Chiolerio A, Digregorio G, Frascella F, Soster M, Bussolino F, Marchiò S, Geobaldo F, Giorgis F (2012) *J Raman Spectrosc* 43:730
- Chiolerio A, Virga A, Pandolfi P, Martino P, Rivolo P, Geobaldo F, Giorgis F (2012) *Nanoscale Res Lett* 7:502
- Yu W, Zhao Z, Zheng W, Long B, Jiang Q, Li G, Ji X (2009) *Polym Eng Sci* 49:491
- Gregorio JRR, Borges DS (2008) *Polymers* 49:4009
- Su J, Kim CH, Kugel VD, Zhang QM, Ting RY, Capps R (2008) *Proceedings of the tenth IEEE international symposium on* 2:927